

## Short Communication

# High-Resolution Mapping of Wet Terrain within Discontinuous Permafrost using LiDAR Intensity

Christopher W. Stevens<sup>1</sup> and Stephen A. Wolfe<sup>2,3\*</sup>

<sup>1</sup> SRK Consulting (US) Inc., Anchorage, Alaska, USA

<sup>2</sup> Natural Resources Canada, Geological Survey of Canada, Ottawa, Ontario, Canada

<sup>3</sup> Department of Geography and Environmental Studies, Carleton University, Ottawa, Ontario, Canada

### ABSTRACT

Surface hydrology is an important aspect of northern environments on account of the thermal influence of water on permafrost. In this study, we demonstrate the ability of light detection and ranging (LiDAR) to map wet terrain within an area of discontinuous permafrost adjacent to the Northwest Territories Highway 3, located west of Yellowknife, Canada. Wet terrain was identified from LiDAR intensity measurements beneath forest canopies and across vegetated surfaces, including peatlands, fens, flooded black spruce and birch forests, and terrain adjacent to the highway embankment. Surface water pathways representing hydrological connections between water bodies and wet terrain were also identified at locations otherwise indiscernible from optical imagery. Statistical separability between terrain types, and thus the ability to map them, was improved by integrating LiDAR all-return and bare-earth intensity with colour orthophotos. The average classification accuracy for wet terrain was 93 per cent. These results indicate that LiDAR intensity can be used for local-scale mapping of wet terrain, as required by northern engineers and scientists. Future integration of LiDAR intensity and elevation measurements may be used to assess changes in surface hydrological conditions impacting permafrost. Copyright © Her Majesty the Queen in Right of Canada 2012.

KEY WORDS: LiDAR intensity; permafrost; hydrology; wet terrain; northern infrastructure; transportation corridor

### INTRODUCTION

Saturated terrain and accumulated surface water are widespread across northern landscapes and cause local warming of the ground (Lachenbruch *et al.*, 1962). The unique thermal properties of water, mainly the large heat capacity and latent heat of fusion, influence aspects of active-layer thaw (Hayashi *et al.*, 2007; Wright *et al.*, 2009) and freezeback (Osterkamp and Romanovsky, 1997), which, in turn, impact heat exchange with the underlying permafrost. Increased surface wetness across poorly drained terrain represents locations where permafrost, if present, may degrade. Thawing of ice-rich permafrost impacts terrain stability (Mackay, 1970; Kokelj *et al.*, 2009) and landscape ecology (Jorgenson *et al.*, 2001; Jorgenson and Osterkamp, 2005). Over time, settlement of the ground surface may increase the accumulation of water and perpetuate local permafrost degradation.

Northern highways represent one form of human modification to the landscape which impedes the movement of surface water. Drainage of water adjacent to roads and highways is of concern to the stability of embankments because of the potential loss of bearing strength and ground settlement associated with the thawing of ice-rich permafrost (Andersland and Landanyi, 2004; Fortier *et al.*, 2011). Stability issues related to permafrost commonly increase annual maintenance costs and decrease the safety of northern transportation infrastructure. Consequently, there is growing interest to utilise remote sensing techniques to assess environmental changes that impact permafrost.

Remote-sensing techniques have recently been used for indirect mapping of permafrost (Nguyen *et al.*, 2009; Panda *et al.*, 2010), land-surface temperature (Han *et al.*, 2004; Hachem *et al.*, 2009) and environmental controls on permafrost processes (Stow *et al.*, 2004; Kääb, 2008; Chasmer *et al.*, 2011; Lui *et al.*, 2012). Among remote-sensing techniques, airborne light detection and ranging (LiDAR) is widely used for acquiring high-resolution terrain elevations primarily along northern

\* Correspondence to: S. A. Wolfe, Natural Resources Canada, Geological Survey of Canada, 601 Booth St, Ottawa, Ontario K1A 0E8, Canada. E-mail: swolfe@NRCan.gc.ca

infrastructure corridors, including pipelines and roads. However, these datasets have been underutilised in terms of signal intensity that can be used for terrain mapping. LiDAR intensity represents the energy returned to the sensor relative to the amount of energy initially transmitted. LiDAR signal intensity measurements have only recently been used for terrain characterisation (Hopkinson, 2007; Mazzarini *et al.*, 2007; Antonarakis *et al.*, 2008) and moisture mapping in low-latitude environments (Garroway *et al.*, 2011). In this paper, we demonstrate the ability of LiDAR intensity to map wet terrain within discontinuous permafrost under forested and non-forested conditions in the context of its thermal impact on permafrost. We define wet terrain hydrologically as saturated ground with bulk water at the surface.

## CASE STUDY AND METHODS

### Highway 3 Corridor

A case study is presented for the Northwest Territories (NWT) Highway 3, west of Yellowknife, where permafrost-hydrological interactions are impacting infrastructure stability (Figure 1). NWT Highway 3 is a major transportation route that services northern communities and mining industries in the region. The highway was constructed between 1999 and 2006 across discontinuous permafrost as part of an upgrade to improve the safety and reliability of the existing transportation infrastructure. The re-built highway, constructed of blast rock with a chip-seal surface, extends across varying terrain units, including black spruce

and birch forest, crystalline bedrock and organic-rich wetlands and bogs. Average annual permafrost temperatures have been reported to be  $> -1.9^{\circ}\text{C}$  in undisturbed peatlands (Karunaratne *et al.*, 2008) and  $> -1^{\circ}\text{C}$  (measured from May-July) beneath the embankment of Highway 3 (EBA Engineering Consultants Ltd, 2003). Ice-rich glaciolacustrine silt and clay with high thaw strains have also been confirmed from boreholes drilled between Yellowknife and Behchoko (EBA Engineering Consultants Ltd, 1995). It is believed that thermal disturbance of ice-rich permafrost along poorly drained sections of the highway has contributed to differential settlement of the embankment (Hoeve *et al.*, 2004).

### LiDAR Data Collection and Processing

LiDAR data presented in this study were collected from a Piper Navajo fixed-wing aircraft, using a Leica ALS50-II with MPiA on the 22 and 24 August 2010 by McElhanney Consulting Services Ltd. The discrete-return system operates in the near-infrared (NIR) spectrum with a laser wavelength of  $1.064\ \mu\text{m}$ , making the intensity of the signal sensitive to water. Survey acquisition parameters for this dataset are presented in Table 1. Colour airphotos were also acquired during the LiDAR survey using a Trimble RolleiMetric AIC P65+ with a 60-mega pixel sensor to produce 20-cm resolution RGB photos. Airphoto orthorectification was performed by McElhanney Consulting Services Ltd.

The LiDAR point cloud data were classified into bare-earth returns using Microstation (v8), TerraScan and TerraModeler software. TerraScan software has been shown to produce results comparable to other classification algorithms (Tinkham *et al.*, 2012), and is based on an iterative process

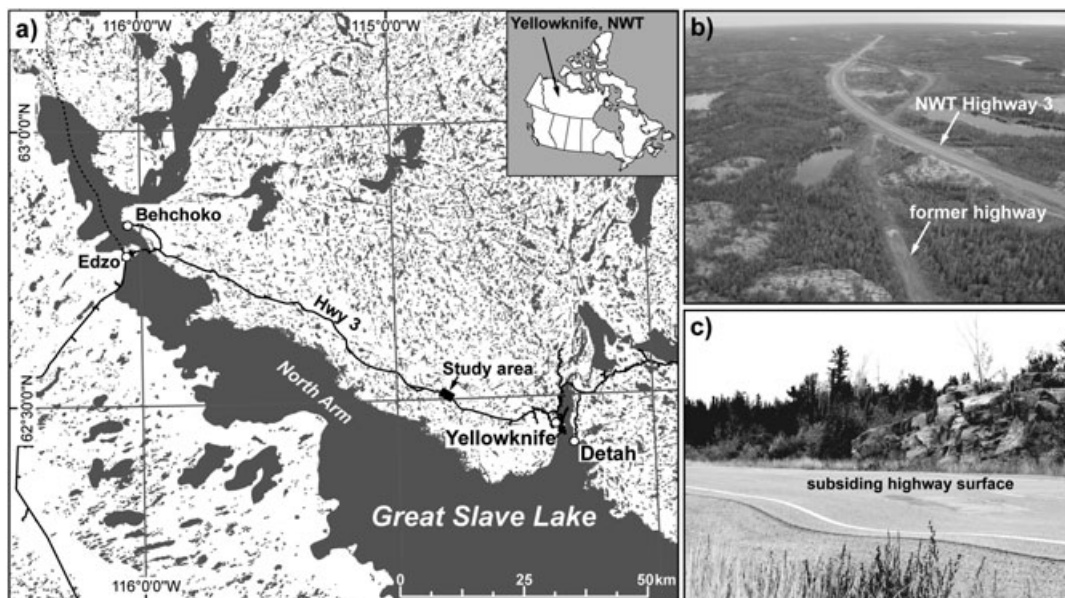


Figure 1 (a) Map showing the study area along Highway 3 located to the west of Yellowknife, Northwest Territories (NWT), Canada. (b) Oblique aerial photograph of the NWT Highway 3 and the former highway. (c) Photograph of differential subsidence of the road embankment along Highway 3.

Table 1 Light detection and ranging survey parameters for data acquired along the Northwest Territories Highway 3.

Acquisition parameter	Value
Survey altitude	1320 m AGL
Laser pulse rate	150 kHz
Scan angle	+/-15°
Swath width	710 m
Swath overlap	30%
Footprint at nadir	0.29 m
Average point density	2.24 pts/m <sup>2</sup>

that generates a ground surface from localised low points, maximum terrain angle and point separation. The mean intensity over 1 m<sup>2</sup> was derived from the point cloud data to produce an eight-bit raster image (digital numbers scaled from 0 to 255).

Intensity measurements presented were not normalised for range bias and atmospheric effects (Hopkinson, 2007), owing to (i) the short acquisition period (2 h), (ii) the relatively flat surface conditions, (iii) the narrow scan width and (iv) the consistency in system parameters. Normalisation of LiDAR data for the above factors reduces intensity variation spatially across the laser scan and where multiple swaths are merged (Hofle and Pfeifer, 2007), potentially resulting in improved terrain classification (Gatziolis, 2009). In this study, LiDAR data were analysed over one swath and local intensity variations were not observed. The main difference in LiDAR intensity for this dataset is expected to relate to changes in surface conditions (roughness and absorption characteristics), which influence the backscatter of energy.

The intensity measurements were examined in terms of 'all returns' ( $I_{AR}$ ) and 'bare-earth returns' ( $I_{BE}$ ). The former represent the laser returns that are reflected from the vegetation canopy (leaves, needles, branches) and/or from the terrain surface. This contrasts with  $I_{BE}$ , which do not include the surface vegetation cover and are solely from the terrain surface. Colour RGB orthophotos were resampled to 1-m spatial resolution using nearest neighbour to allow for direct comparison with LiDAR  $I_{AR}$  and  $I_{BE}$  images. Representative terrain types were chosen on the basis of our field experience within the study area. The separability of each terrain type was assessed using a transformed divergence (TD) statistic, which is a measure of the distance between mean reflectance values in the N-dimensional space (Richards, 1986).

Supervised classification of wet terrain was performed using the LiDAR  $I_{AR}$  and  $I_{BE}$  images and the three RGB orthophoto bands (total of 5 data bands). Training data for the classification included five terrain classes established from field observations and airphoto interpretation: (1) highway surface (n = 760); (2) exposed bedrock (n = 1060); (3) forested terrain (n = 826); (4) dry organic terrain (n = 878); and (5) wet terrain and water bodies (n = 1904). A maximum likelihood classification was run

over 20 repeat iterations using a random selection of 40 per cent of the training data points following the procedure of Harris *et al.* (2012). The remaining 60 per cent of the training data were used to assess the classification accuracy. We present the average accuracy and the majority classification image over the 20 iterations.

## RESULTS AND DISCUSSION

### LiDAR $I_{AR}$ and $I_{BE}$

Figure 2 shows LiDAR  $I_{AR}$  and  $I_{BE}$  images and corresponding colour orthophotos along a section of Highway 3. The intensity measurements vary across the landscape in response to changes in terrain type, vegetation cover (species type and density) and surface moisture, which are attributed to differences in surface roughness and absorption characteristics. The LiDAR  $I_{AR}$  image (Figure 2c) indicates high spatial variability in intensity caused by laser returns that are reflected from the high-intensity (bright tone) bare-earth surface, moderate-intensity vegetation canopy and low-intensity (dark tone) wet terrain. Wet terrain is more clearly recognised in the LiDAR  $I_{BE}$  image (Figure 2d), where laser returns from the vegetation canopy have been removed. However, vegetated terrain type is poorly differentiated in the  $I_{BE}$  image because of the similarity in surface intensity. As a result, the  $I_{AR}$  image is important in identifying various types of vegetated terrain and the  $I_{BE}$  image is more effective in identifying wet terrain.

The distribution of LiDAR  $I_{AR}$  and  $I_{BE}$  for representative terrain types in this region is shown in Figure 3. For exposed terrain with limited or no surface vegetation (i.e. vegetation canopy or understory), the  $I_{AR}$  is equal or nearly equal to the  $I_{BE}$ , as the first and second laser returns are largely from the bare-earth surface. These terrain types include the highway surface, dry open peatlands and exposed bedrock, which on average plot along the 1:1 line (Figure 3b). For forested terrain, the  $I_{AR}$  (mean = 91,  $\sigma = 45$ ) and  $I_{BE}$  (mean = 159,  $\sigma = 21$ ) are unequal because of the influence of the vegetation canopy within the former grouping. The unequal  $I_{AR}$  and  $I_{BE}$  response for wet terrain is similarly caused by laser returns from the vegetation canopy at sites where the forest has been inundated by water (Figure 3). The average  $I_{AR}$  is 40 ( $\sigma = 33$ ) and the  $I_{BE}$  is 18 ( $\sigma = 13$ ) for flooded forested terrain. For open bodies of water and wetlands with limited vegetation cover, the average  $I_{AR}$  and  $I_{BE}$  also plot along the 1:1 line.

Low  $I_{BE}$  values associated with wet terrain are caused by the absorption of the transmitted NIR energy. Where present, aquatic vegetation on the water surface produces slightly higher intensity returns. In some cases, the smooth water surface also acts as a specular reflector over larger ponds and no laser return is measured. High-intensity values caused by specular reflection at nadir were not observed, but represent a source of higher intensity from water (Hopkinson *et al.*, 2011).

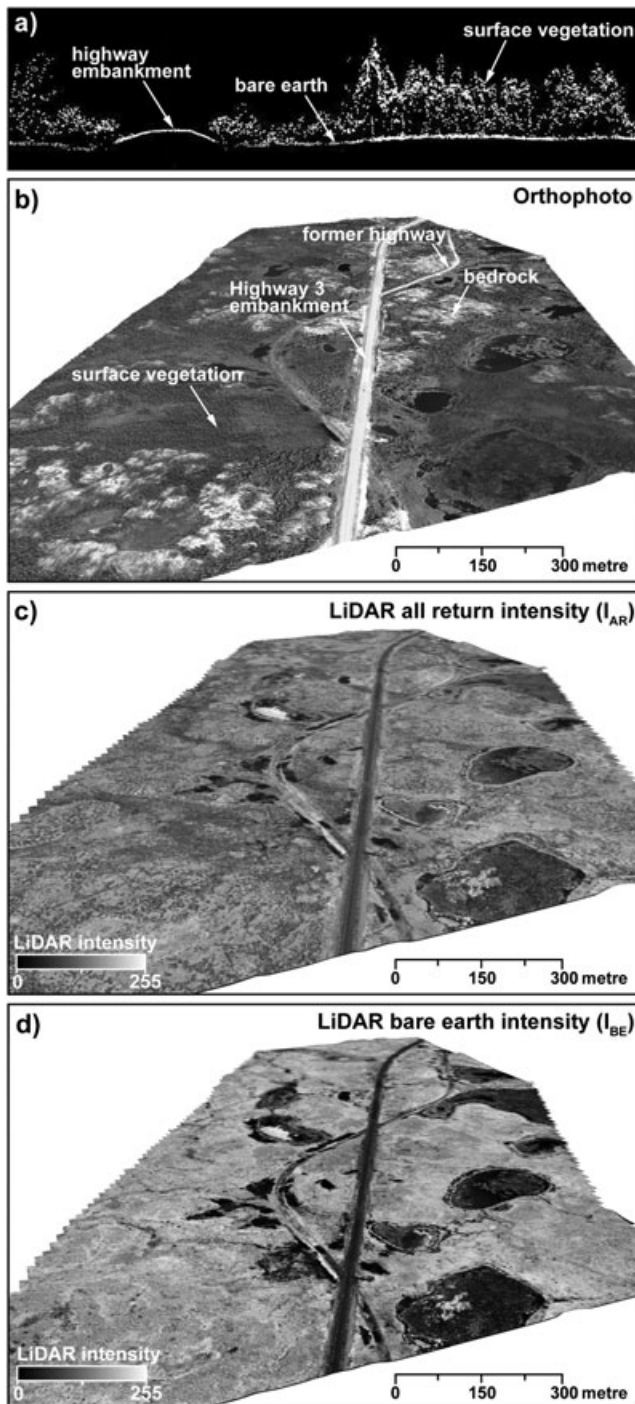


Figure 2 (a) Cross-sectional view of light detection and ranging (LiDAR) point cloud (all returns). Oblique view of: (b) colour RGB orthophoto converted to grey scale; (c) LiDAR all-return intensity ( $I_{AR}$ ); and (d) LiDAR bare-earth intensity ( $I_{BE}$ ) images.

### Statistical Separability of Wet Terrain

Statistical separability based on the transformed divergence of each terrain type using colour RGB orthophotos and LiDAR  $I_{AR}$  and  $I_{BE}$  is presented in Table 2. The calculated

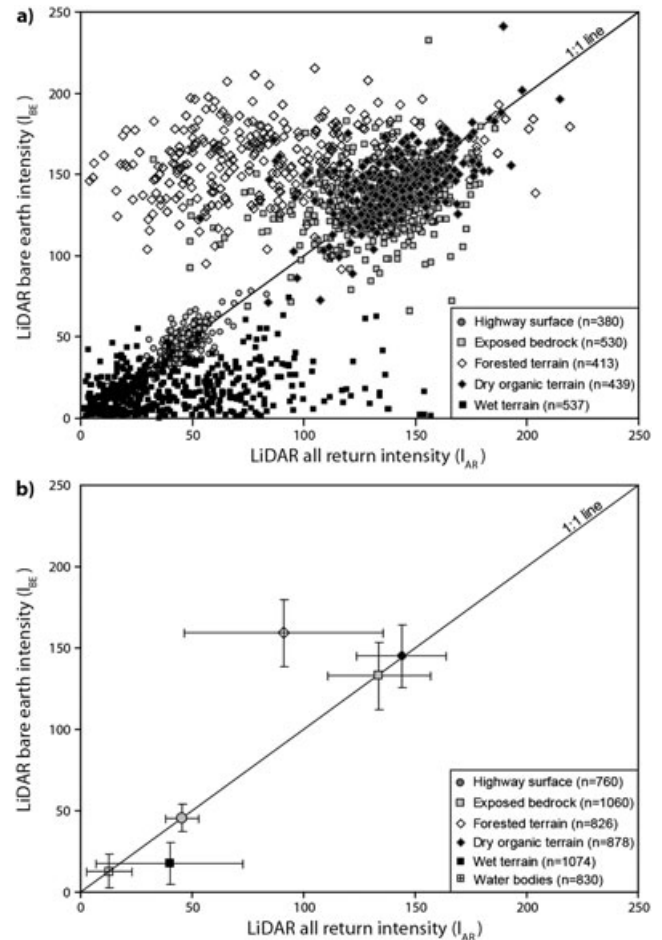


Figure 3 (a) Light detection and ranging (LiDAR) all-return intensity ( $I_{AR}$ ) and bare-earth intensity ( $I_{BE}$ ) for major terrain types along the NWT Highway 3 corridor. The number of intensity measurements shown is reduced for clarity. (b) Mean LiDAR intensity (symbol) and standard deviation  $1\sigma$  (bars) for each terrain type.

separability is used to assess the distinction between terrain types using the available data. Terrain types with a low separability have similar traits (signatures), resulting in the potential for misclassification and inaccurate mapping.

Spectral information from RGB orthophotos provides good-to-moderate separability ( $TD > 1.5$ ) between each terrain type, with the exception of wet terrain (Table 2). The poor separability ( $TD < 1.5$ ) of wet terrain is caused by the presence of surface vegetation, which provides the dominate response back to the camera sensor. This limits the ability to distinguish spectrally wet terrain below the forest canopy and across vegetated surfaces using RGB orthophotos. Similarly, poor separability of dry organic, exposed bedrock and forested terrain exists when solely relying on LiDAR intensity because of terrain similarities in intensity measurements (Table 2; Figure 3). As a result, overall terrain separability and thus accurate mapping of these terrain types are improved by combining canopy and surface information obtained from both colour orthophotos and LiDAR intensity images (Table 2).

Table 2 Transformed divergence (TD) statistics calculated for each terrain type using colour RGB orthophotos and light detection and ranging all-return intensity ( $I_{AR}$ ) and bare-earth intensity ( $I_{BE}$ ).

Terrain type	TD (RGB)	TD ( $I_{AR}$ , $I_{BE}$ )	TD ( $I_{AR}$ , $I_{BE}$ , RGB)
Dry organic vs bedrock	1.65	<b>0.14</b>	1.71
Forested terrain vs bedrock	1.86	<b>0.95</b>	1.93
Dry organic vs forested terrain	1.67	<b>0.99</b>	1.84
Wet terrain vs highway surface	2.00	<b>1.22</b>	2.00
Wet terrain vs bedrock	1.64	1.90	1.98
Wet terrain vs dry organic	<b>0.64</b>	1.96	1.97
Wet terrain vs forested terrain	<b>0.95</b>	1.97	1.99
Bedrock vs highway surface	<b>1.32</b>	1.99	2.00
Forested terrain vs highway surface	2.00	2.00	2.00
Dry organic vs highway surface	2.00	2.00	2.00

Note: Numbers highlighted in bold represent terrain types with poor separability (TD < 1.5 out of 2.0).

Integration of both data sources produces an average classification accuracy of 95 per cent using the major terrain types (kappa coefficient of 0.93). Wet-terrain classification has an average accuracy of 93 per cent, consistent with field observations. Terrain classification may be improved with the use of LiDAR elevation and its derivative measurements (i.e. slope, roughness, curvature). In particular, wet terrain may exhibit low surface roughness and low local variability in  $I_{BE}$  that enhance mapping. In addition, outputs generated from hydrological surface models, such as wetness indices and flow accumulation networks, have the potential to verify the location and connectivity of wet terrain across the landscape.

### Wet Terrain along Highway 3 Corridor

Figure 4 shows a section of the Highway 3 corridor where wet terrain has been mapped using LiDAR intensity and colour orthophotos. Wet terrain is identified across fens, bogs and peatlands where wet surfaces naturally occur, and mixed black spruce and birch forests are identified that have been inundated by water. Surface water pathways representing the hydrological connection between water bodies and wet terrain are also evident from the  $I_{BE}$  image and classified map (Figure 4c, d). These pathways are not easily identified from aerial surveys or photographs because of the obscuring tree canopy and low-lying vegetation cover.

Adjacent to the Highway 3 embankment, surface water is present where topographic depressions have formed and poor drainage exists (Figure 4d). A large portion of the wet terrain occurs on the north side of the embankment, representing the upslope side of the natural north-to-south direction of drainage. At these locations, the impact of changing surface hydrology may be perceived by the presence of dead black spruce and birch trees adjacent to the highway corridor (Figure 4a, c). Wet terrain and surface water are also identified along abandoned sections of the former highway.

The warm discontinuous permafrost ( $> -1^{\circ}\text{C}$ ) along the highway corridor is susceptible to thaw where changes in surface hydrology alter the surface energy budget and the

thermal properties of the ground. Water-jet boreholes drilled in 2010 within the right-of-way indicate that permafrost beneath disturbed terrain exhibits deep thaw depths or is absent (Figure 4a). As a result, wet-terrain mapping from LiDAR identifies sites where permafrost disturbance may be caused by water. The thawing of ice-rich permafrost initiated by surface hydrology changes may result in settlement and increased surface wetness that perpetuate local permafrost degradation. The potential for advective heat transfer associated with ground water movement also exists (de Grandpre *et al.*, 2012).

### CONCLUSIONS

This case study indicates that LiDAR intensity measurements can be used to map wet terrain because of the sensitivity of the transmitted NIR energy to surface water. The following conclusions are reached about the wet terrain adjacent to the NWT Highway 3:

1. LiDAR intensity provides high-resolution detection of wet terrain across forested and non-forested surfaces, making it a useful tool for mapping surface hydrology within discontinuous permafrost.
2. Wet terrain identified from LiDAR  $I_{BE}$  images corresponds to wet peatlands and fens, flooded black spruce and birch forest, and locations where water has accumulated adjacent to the highway infrastructure. Surface water pathways representing the hydrologic connection between water bodies and wet terrain were also identified at locations otherwise indiscernible from optical imagery.
3. Terrain classification was improved upon by combining colour orthophotos and LiDAR  $I_{AR}$  and  $I_{BE}$ , owing to the increased separability achieved through characterising the spectral response from both the vegetation canopy and the bare-earth surface. The average classification accuracy of wet terrain was 93 per cent.

In short, mapping of wet terrain using LiDAR intensity measurements provides both a potentially valuable tool for

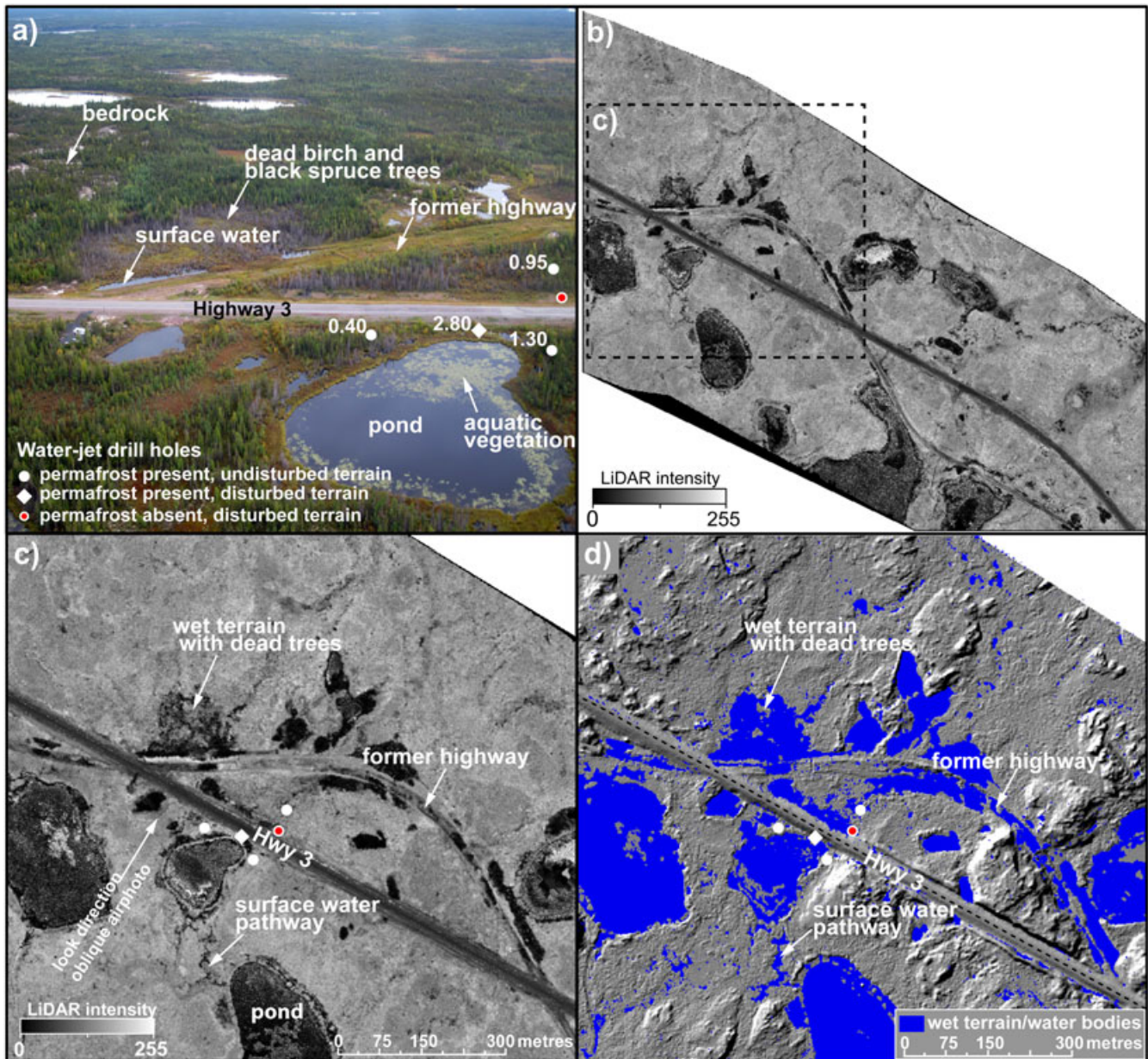


Figure 4 (a) Oblique aerial photograph showing wet terrain adjacent to the Northwest Territories Highway 3. (b, c) Light detection and ranging (LiDAR) bare-earth intensity images showing low-intensity areas associated with wet terrain. (d) Majority classification of wet terrain and water bodies (blue) produced from the integration of LiDAR intensity and RGB orthophoto measurements. Solid dots indicate the presence or absence of permafrost based on water-jet boreholes drilled in 2010. Numbers indicate thaw depth in metres. This figure is available in colour online at [wileyonlinelibrary.com/journal/ppp](http://wileyonlinelibrary.com/journal/ppp)

terrain assessment and an improved understanding of local factors that affect permafrost stability. LiDAR mapping applied to infrastructure corridors can identify locations where permafrost may be thermally disturbed by surface water and where additional drainage measures are required. Combined with field-level data, LiDAR range and intensity measurements can provide new insight into related changes in surface elevation, hydrology and permafrost.

## ACKNOWLEDGEMENTS

This work is a contribution to the Great Slave Transportation Risk in the Arctic to Climatic Sensitivity activity within the Climate Change Geoscience Program of Natural Resources Canada, and represents Geological Survey of Canada contribution number 20120015. We acknowledge support from the Geomapping for Energy and Minerals Program for

purchase of the LiDAR data. This paper was developed during CWS's term as a Natural Science and Engineering Research Council of Canada visiting fellow with Natural

Resources Canada. This paper benefited from comments by Caroline Duchesne, Greg Brooks, two anonymous reviewers and the journal Editors.

## REFERENCES

- Andersland OB, Landanyi B. 2004. *Frozen Ground Engineering*, Second Edition. John Wiley & Sons, Inc: New Jersey; 363pp.
- Antonarakis AS, Richards KS, Brasinton J. 2008. Object-based land cover classification using airborne lidar. *Remote Sensing of Environment* **112**: 2988–2998. DOI: 10.1016/j.rse.2008.02.004
- Chasmer L, Quinton W, Hopkinson C, Petrone R, Whittington P. 2011. Vegetation canopy and radiation controls on permafrost plateau evolution within the discontinuous permafrost zone, Northwest Territories, Canada. *Permafrost and Periglacial Processes* **22**: 199–213. DOI: 10.1002/ppp.724
- de Grandpre I, Fortier D, Stephani E. 2012. Degradation of permafrost beneath a road embankment enhanced by heat advected in groundwater. *Canadian Journal of Earth Sciences* **49**: 953–962. DOI: 10.1139/E2012-018
- EBA Engineering Consultants Limited. 1995. Yellowknife Highway (No. 3), N.W.T. km 242 to km 256. Preliminary Geotechnical Evaluation. Report 0701-95-11776, 130pp.
- EBA Engineering Consultants Limited. 2003. Preliminary Geothermal Evaluation of Yellowknife Highway (NWT No. 3) Km 252+680 & Km 262+330. Project 0701–1700051.506, 28pp.
- Fortier R, LeBlanc A-M, Yu W. 2011. Impacts of permafrost degradation on a road embankment at Umiujaq in Nunavik (Quebec), Canada. *Canadian Journal of Earth Sciences* **48**: 720–740. DOI: 10.1139/T10-101
- Garroway K, Hopkinson C, Jamieson R. 2011. Surface moisture and vegetation influences on lidar intensity data in an agricultural watershed. *Canadian Journal of Remote Sensing* **37**: 275–284. DOI: 10.5589/m11-036
- Gatziolis D. 2009. LiDAR intensity normalization in rugged forested terrain. In *Proceedings of Silvilaser 2009 - The 9th international conference on lidar applications for assessing forest ecosystems*, Popescu SC, Nelson R, Zhao K, Neuenschwander A (eds). Texas A & M University College Station: Texas, USA, 14–16 October, 8pp.
- Hachem S, Allard M, Duguay C. 2009. Using the MODIS land surface temperature product for mapping permafrost: an application to Northern Quebec and Labrador, Canada. *Permafrost and Periglacial Processes* **20**: 407–416. DOI: 10.1002/ppp.672
- Han K-S, Viau AA, Anctil F. 2004. An analysis of GOES and NOAA derived land surface temperatures estimated over a boreal forest. *International Journal of Remote Sensing* **25**: 4761–4780. DOI: 10.1080/01431160410001680446
- Harris JR, He J, Grunsky E, Gorodetzky D, Brown N. 2012. A robust, cross validation classification method (RCM) for improved mapping accuracy and confidence metrics. *Canadian Journal of Remote Sensing* **38**: 69–90. DOI: 10.5589/m12-013
- Hayashi M, Goeller NT, Quinton WL, Wright N. 2007. A simple heat-conduction method for simulating the frost-table depth in hydrological models. *Hydrological Processes* **21**: 2610–2622. DOI: 10.1002/hyp.6792
- Hoeve TE, Seto JTC, Hayley D. 2004. Permafrost response following reconstruction on the Yellowknife highway. In *International Conference on Cold Regions Engineering*, Edmonton. American Society of Civil Engineers: Reston, Virginia, USA; 5pp.
- Hofle B, Pfeifer N. 2007. Correction of laser scanning intensity data: Date and model-driven approaches. *Journal of Photogrammetry and Remote Sensing* **62**: 415–433. DOI: 10.1016/j.isprsjprs.2007.05.008
- Hopkinson C. 2007. The influence of flying altitude, beam divergence, and pulse repetition frequency on laser pulse return intensity and canopy frequency distribution. *Canadian Journal of Remote Sensing* **33**: 312–324. DOI: 10.5589/m07-029
- Hopkinson C, Crasto N, Marsh P, Forbes D, Lesack L. 2011. Investigating the spatial distribution of water levels in the Mackenzie Delta using airborne LiDAR. *Hydrological Processes* **25**: 2995–3011. DOI: 10.1002/hyp.8167
- Jorgenson MT, Osterkamp TE. 2005. Response of boreal ecosystems to varying modes of permafrost degradation. *Canadian Journal of Forest Research* **35**: 2100–2111. DOI: 10.1139/x05-153
- Jorgenson MT, Racine CH, Walters JC, Osterkamp TE. 2001. Permafrost degradation and ecological changes associated with a warming climate in central Alaska. *Climatic Change* **48**: 551–579.
- Kääb A. 2008. Remote sensing of permafrost-related problems and hazards. *Permafrost and Periglacial Processes* **19**: 107–136. DOI: 10.1002/ppp
- Karunaratne KC, Kokelj SV, Burn CR. 2008. Near-surface permafrost conditions near Yellowknife, Northwest Territories, Canada. In *Proceedings, Ninth International Conference on Permafrost*, Kane DL, Hinkel KM (eds). University of Alaska Fairbanks: Alaska, USA; 907–912.
- Kokelj SV, Lantz TC, Kanigan J, Smith SL, Coutts R. 2009. Origin and polycyclic behavior of tundra thaw slumps, Mackenzie Delta Region, Northwest Territories, Canada. *Permafrost and Periglacial Processes* **20**: 173–184. DOI: 10.1002/ppp.642
- Lachenbruch AH, Brewer MC, Greene GW, Marshall BV. 1962. Temperatures in permafrost. In *Temperature: Its Measurement and Control in Science and Industry*, Vol. 3, part 1, Herzfeld CM (ed). Reinhold: New York, NY; 791–803.
- Lui L, Schaefer K, Zhang T, Wahr J. 2012. Estimating 1992–2000 average active layer thickness on the Alaskan North Slope from remotely sensed surface subsidence. *Journal of Geophysical Research* **117**: F01005. DOI: 10.1029/2011JF002041
- Mackay JR. 1970. Disturbances to the tundra and forest tundra of the western Arctic. *Canadian Geotechnical Journal* **7**: 420–432.
- Mazzarini F, Pareschi MT, Favalli M, Isola I, Tarquini S, Boschi E. 2007. Lava flow identification and aging by means of LiDAR intensity: Mount Etna case. *Journal of Geophysical Research* **112**: B02201. DOI: 10.1029/2005JB004166
- Nguyen T-N, Burn CR, King DJ, Smith SL. 2009. Estimating the extent of near-surface permafrost using remote sensing, Mackenzie Delta, Northwest Territories. *Permafrost and Periglacial Processes* **20**: 141–153. DOI: 10.1002/ppp.637
- Osterkamp TE, Romanovsky VE. 1997. Freezing of the active layer on the coastal plain of the Alaskan Arctic. *Permafrost and Periglacial Processes* **8**: 23–44.
- Panda SK, Prakash A, Solie DN, Romanovsky VE, Jorgenson MT. 2010. Remote sensing and field-based mapping of permafrost distribution along the Alaska Highway corridor, interior Alaska. *Permafrost and Periglacial Processes* **21**: 271–281. DOI: 10.1002/ppp.686
- Richards JA. 1986. *Remote Sensing Digital Image Analysis*. Springer-Verlag: Berlin, Heidelberg, New York, London, Paris, Tokyo.
- Stow DA, Hope AS, McGuire D, Verbyla DL, Gamon J, Huemmrich F, Houston S, Racine CH, Sturm M, Tape K, Hinzman LD, Yoshikawa K, Tweedie CE, Noyle B, Silapaswan C, Douglas D, Griffith B, Jia

GJ, Epstein HE, Walker DA, Daeschner S, Petersen A, Zhou L, Myneni RB. 2004. Remote sensing of vegetation and land cover change in arctic tundra ecosystems. *Remote Sensing of Environment* **89**: 281–308. DOI: 10.1016/j.rse.2003.10.018

Tinkham WT, Smith AMS, Hoffman C, Hudak AT, Falkowski MJ, Swanson ME, Gessler PE. 2012. Investigating the influence of LiDAR ground surface errors on the utility of derived forest inventories. *Canadian Journal of Forest Research* **42**: 413–422. DOI: 10.1139/X11-193

Wright N, Hayashi M, Quinton WL. 2009. Spatial and temporal variations in active layer thawing and their implication on runoff generation in peat-covered permafrost terrain. *Water Resources Research* **45**: W05414. DOI: 10.1029/2008WR006880